SUN INDUCES SEMI-DIURNAL STRESSES ON EARTH'S SURFACE, WHICH TRIGGER EARTHQUAKES AND VOLCANIC ERUPTIONS

Vinayak G. Kolvankar
Seismology Division, Bhabha Atomic Research Centre, Trombay, Mumbai 400 085, India
Email: vkolvankar@yahoo.com Fax numbers : +9122 25505151, 25519613

Abstract: Various research workers have reported EM (electro-magnetic) emissions prior to the earthquakes or during earthquake sequences. In some cases these EM emissions were consistently found during certain hours of the day. These were found to be of diurnal and semidiurnal type. EM emissions of semi-diurnal type, spaced in the time domain from the local noontime, were observed in many examples prior to earthquakes/volcanic eruptions. Such emissions were also observed in a very wide frequency band from VLF (very low frequency) to Microwave range. It was also found in these examples that earthquakes/volcanic eruptions occurred simultaneously with these EM emissions. From this study, it can be concluded that the semidiurnal stresses on the earth and moon are primarily caused by the position of the Sun. This paper discusses all these examples in detail and an application for the development of reliable monitoring of precursors for earthquakes/volcanic eruptions in high-seismicity areas.

Keywords: *Telemetered network, semi-diurnal, diurnal RF emission, earthquake sequence and precursors.*

1. INTRODUCTION

Many research workers have reported EM emissions prior to earthquakes and volcanic eruptions. Among these, the semidiurnal type (twice a day) was commonly seen. However, the diurnal type (once a day) of EM emission was also noticed in a few cases.

Both these types of EM emission were observed during the operation of an indigenously built radio telemetered seismic network (RTSN) which was commissioned at Bhatsa (20º 37 N, 73º 18 E), Maharashtra state, India, to study the reservoir-induced seismicity (RIS) of the region and operated during 1989 -1995 (Kolvankar et al.,1992). RF (radio frequency) interference to the radio links operated in the UHF (Ultra High Frequency) band was witnessed prior to, during and after the earthquake sequence from the Valsad region.

The semidiurnal type of EM emission related to earthquakes and volcanic eruptions was also observed in many other cases. Six such prominent examples including that observed at Bhatsa related to the Valsad earthquake sequence (which also showed a diurnal pattern of EM emission) are briefly described below:

2. EXAMPLES OF SEMIDIURNAL TYPE OF EM EMISSION RELATED TO EARTHQUAKES AND VOLCANIC ERUPTIONS

2.1 Example 1: Diurnal and semi-diurnal RF emission related to Valsad earthquake sequence observed at Bhatsa

The RTSN was established at Bhatsa to monitor the reservoir-induced seismicity of the region. This network had 10 field stations spread over an area of around 500 sq. km. Each station had a single vertical seismometer and signal-conditioned analog data from this sensor was frequency modulated and sent to the base station via individual links operated at the spot frequency in the UHF band (461- 462 MHz), on a 24-hour basis. At the base station, the data from this network was edited online and the event portion with about 15 sec. of pre-event portion was recorded on a magnetic tape in digital format (Kolvankar et al., 1992). The layout of the Bhatsa network is shown in Fig. 1.

The network recorded an earthquake sequence from the Valsad region located 115 km north of this network. Nearly 400 events in the magnitude range of 1.4 to 5.0 were recorded from 25 March 1991 to 30 June 1991 with the main event of magnitude 5.0 on 30 April 1991 (05:13:56 GMT).

Three weeks prior to the start of the earthquake sequence, intense diurnal disturbances were witnessed during 5–11 March 1991 only at certain times (close to 00:00 hours GMT). The entire network was disrupted for a few minutes on five different occasions. A specimen of the diurnal-type RF disturbance is provided in Fig. 2. In this

figure only the start portion of the RF disturbance (at 23:57:00 on 8 March 1991) and the end portion (at 00:18:00 on 9 March 1991) are illustrated in separate parts. As illustrated in this figure the end portion of the RF disturbance is an exact mirror replica of the start portion.

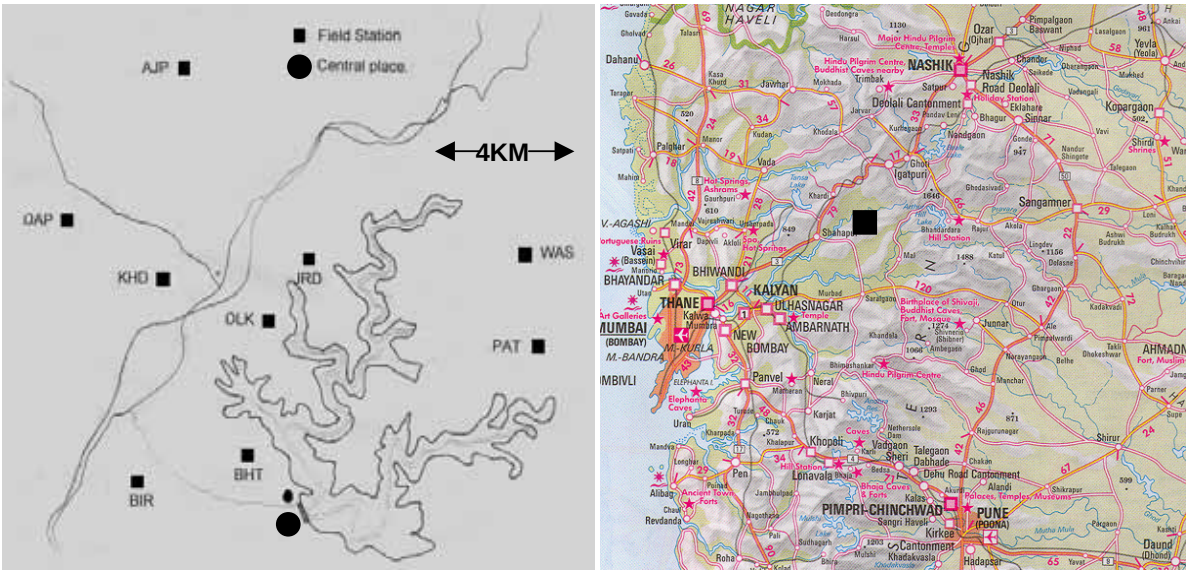

Fig. 1. Layout of the RTSN at Bhatsa, India. Approximate location of the network area is indicated by a black square in the adjacent map

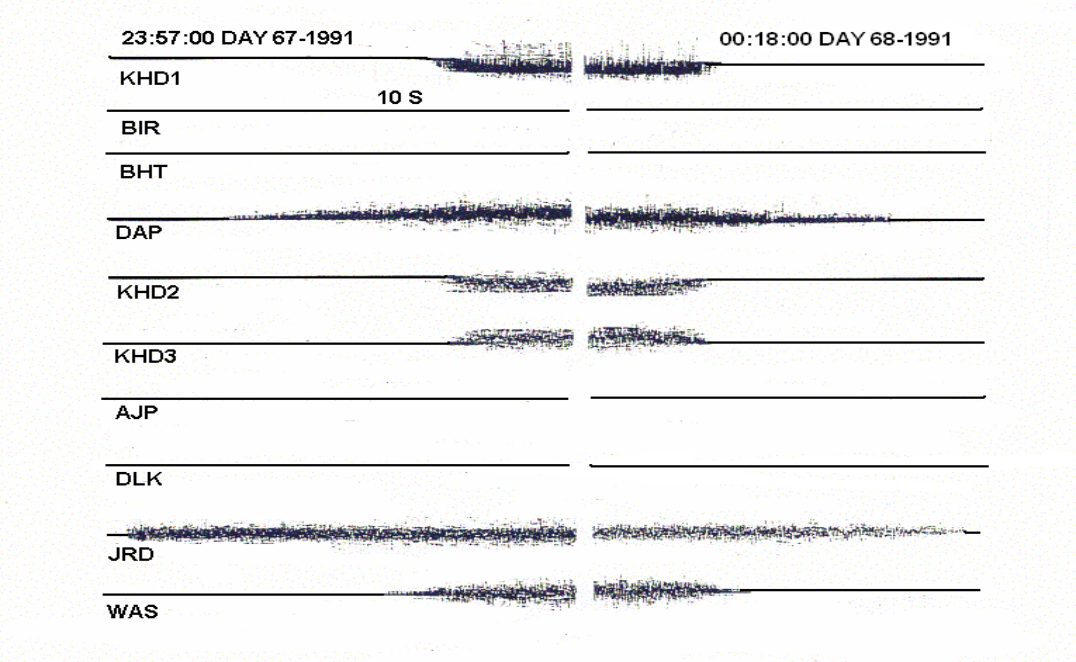

Figure 2: Start portion (23:57:00 on day 67, 8 March 1991) and end portion (00:18:00 on day 68, 9 March 1991) of the RF disturbance are illustrated on multi-channel seismic data at low sensitivity, which normally should provide straight lines. The latter portion is an exact mirror replica of the start portion of this RF disturbance. KHD station had a tri-axial sensor and three-component analog data was telemetered using the FDM (frequency division multiplexing) technique.

Table 1 provides details of the RF disturbance (diurnal type) during the pre-earthquake sequence period. It is evident from this table that for eight consecutive days (barring day 65) the RF disturbance was experienced close to 00 hours (GMT) in most of the RF links of the network. After the start of the earthquake sequence (on 25 March 1991), RF disturbances of the semidiurnal type were observed for about three weeks, only at certain times (04 and 12 hours GMT) of the day and then terminated with the occurrence of the main event on 30 April 1991.

Table 1: Details of the RF disturbance experienced by the Bhatsa network prior to the onset of the Valsad earthquake sequence on 25 March 1991. AJP, PAT, JRD, DAP are the abbreviations of several field stations. The signals from AJP and PAT stations were also monitored on a helical drum recorder on a 24-hour basis.

SER. NO.	DATE [DAY]	TIME	DURATION	REMARKS
1	05.03.91[64]	01:25:20	300 Sec.	Seen in AJP and PAT helical records
2	05.03.91[64]	12:45:30	40 Sec.	**All working channels affected**
3	05.03.91[64]	22:17:06	270 Sec.	Seen in AJP and PAT helical records
4	08.03.91[67]	01.28.10	180 Sec.	**All working channels affected**
5	08.03.91[67]	23:57:00	7.5 – 23 Min.	**All working channels affected**
6	09.03.91[68]	23:56:30	22 Min.	**All working channels affected**
7	10.03.91[69]	00:37:00	120 Sec.	Multi-channel play-out available
8	10.03.91[69]	23:53:20	100 Sec.	Seen in AJP helical records
9	11.03.91[70]	23:56:00	13 Min.	**All working channels affected**

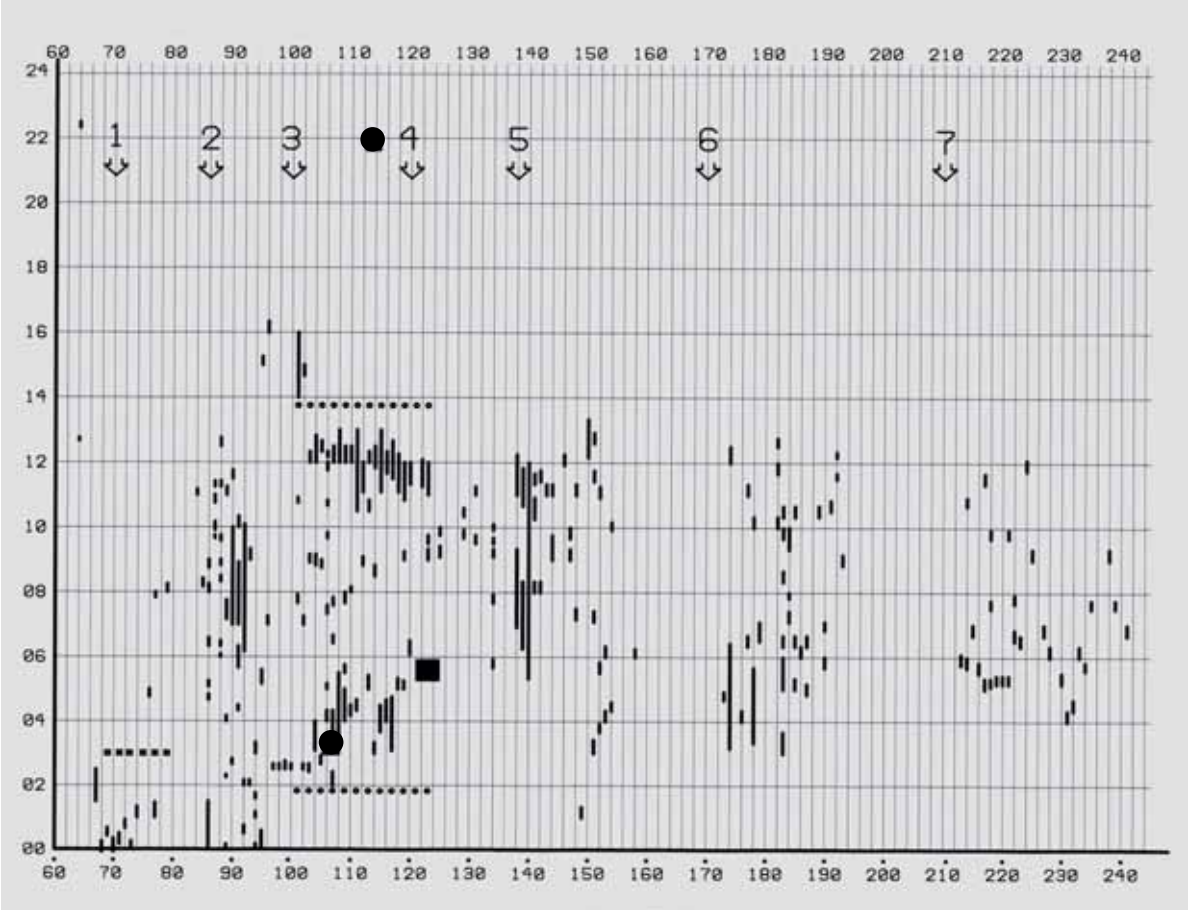

Figure 3: Picture of the RF disturbance for the period from 1 March (day 60) till the end of August 1991. In this figure each vertical line represents a day and it is segmented every 2 hours. For convenience, vertical lines are shown for alternate days. Thick lines indicate the RF activities and their lengths indicate the duration. To produce a visible display, longer lines are drawn for short-duration disturbances (in the order of few seconds). Positions of two major foreshocks are shown with circular dots and that of the main event with a square dot. The timings of the main event and one of the foreshock match the timings of the EM emission at around 0400 hours [GMT]. **(The semi-diurnal portion of the RF disturbance is indicated within a pair of circular dotted lines, whereas the diurnal portion is indicated under a square dotted line.)**
The arrows indicate the following:
Arrow 1: Start of the RF disturbance in the radio links at around 00 hours GMT.
Arrow 2: Start of the earthquake sequence.
Arrow 3: Occurrence of major foreshock, RF disturbance shifted to around 04 and 12 hours GMT.
Arrow 4: Occurrence of main shock of Mg. 5.0. RF disturbance pattern changes.
Arrows 5 and 6: RF disturbances associated with few aftershocks of Mg. 2.5-3.5.
Arrow 7: End of earthquake sequence. However RF disturbance continued in patches for 2 months.

After the onset of the earthquake sequence, the RF disturbances observed were of much longer duration extending to over 100 minutes and were confined to the disturbances of telemetry links from stations situated in the northern region only. Only the receivers with antennas pointing towards north were affected by these disturbances. However in cases of RF disturbances prior to the occurrence of the Valsad earthquake sequence, it was observed that most RF links were affected, which include stations in the east and west directions indicating that they must have been much stronger than the RF disturbances experienced when the earthquake sequence was in progress.

Fig. 3 provides an overall picture of the RF disturbance for period from 1 March (day 60) till the end of August 1991. The caption to this figure provides details of the overall RF disturbance experienced by this network. The details of the Valsad earthquake sequence are provided elsewhere (Kolvankar et al., 2001).

2.2 Example 2: Volcanic Eruption at Mt. Mihara

Yoshino and Tomizawa (1989) observed low-frequency (82 kHz) EM emissions at precursors to the volcanic eruption at Mt. Mihara during Nov. 1986. Volcanic micro-vibrations were observed at Oshima observatory from July 1986 onward but the anomalous impulsive noise emission at 82 kHz did not appear until after Oct. 20. Several clear burst-like emissions were gathered during Nov. 3 to 22. The times of the bursts are provided in table 2. It can be seen that the EM emissions were confined to 09 to 11 and 14 to 16 hours (JST) only. Also the timings of the first eruption in creator A (at 17:25 hours on Nov. 15, 1986) and the simultaneous eruption in creator C (at 16:21 hours on 21 Nov 1986) match the timings of the EM emission observed.

Table 2. The timings of the low-frequency (82 kHz) EM emissions, which were probable precursors to the volcanic eruption at Mt. Mihara during Nov. 1986.

DAY	EM EMISSION TIMINGS [JST]	REMARKS
Nov 3	14-16	
Nov 4	09-11 16	
Nov 8	11:30 14-16	
Nov 10	09	
Nov11	11	
Nov 14	11 to 16 (continuous)	A major emission a day before the first eruption
Nov 15		At 17:25, **first eruption.** No emission observed. Lava fountains [200 m high] were witnessed at crater A. The earthquake and volcanic micro-vibration continued during the eruption.
Nov 17	8-9 14-15	Emissions were observed
Nov 19		**At 23 JST eruption ceased.**
Nov 21	10-12	Strong emission, strong local earthquakes.
Nov 21	10-12	Emissions were observed.
Nov 21		**At 16:15, simultaneous eruption in crater C Lava fell on the observatory destroying all equipment**

2.3 Example 3: Great Chilean earthquake of 1960

Part A of Fig. 4 shows the relative position of observation posts during the recording of anomalous effects of the Alaskan earthquake (28.03.1964, Mb = 8.3) and that of the Chilean earthquake (22.05.1960, Mb = 8.5). Part B of the same figure shows the recording of diurnal signal intensity envelopes at a frequency of 10 MHz on the Washington-Huankayo path prior to the disastrous quake in Chile. This intensity envelope has a pronounced 24-hour variation in the shape of a wave minimum at 14-21 hours UT (day interval) and maximum 23-11 hours (night interval), mainly caused by ionosphere changes with the signal gradually rising over 20-00 hours and decreasing over 11-14 hours. 2.5 days prior to the main earthquake, the signal during the nights of 19, 20 and 21 May went off the scale (as seen from the saturated output). As seen in part B of this figure, an hour before the first foreshock on 21 May, the signal tends to return to the background level and again goes off the scale at the time of the earthquake (Gokhberg et al., 1995).

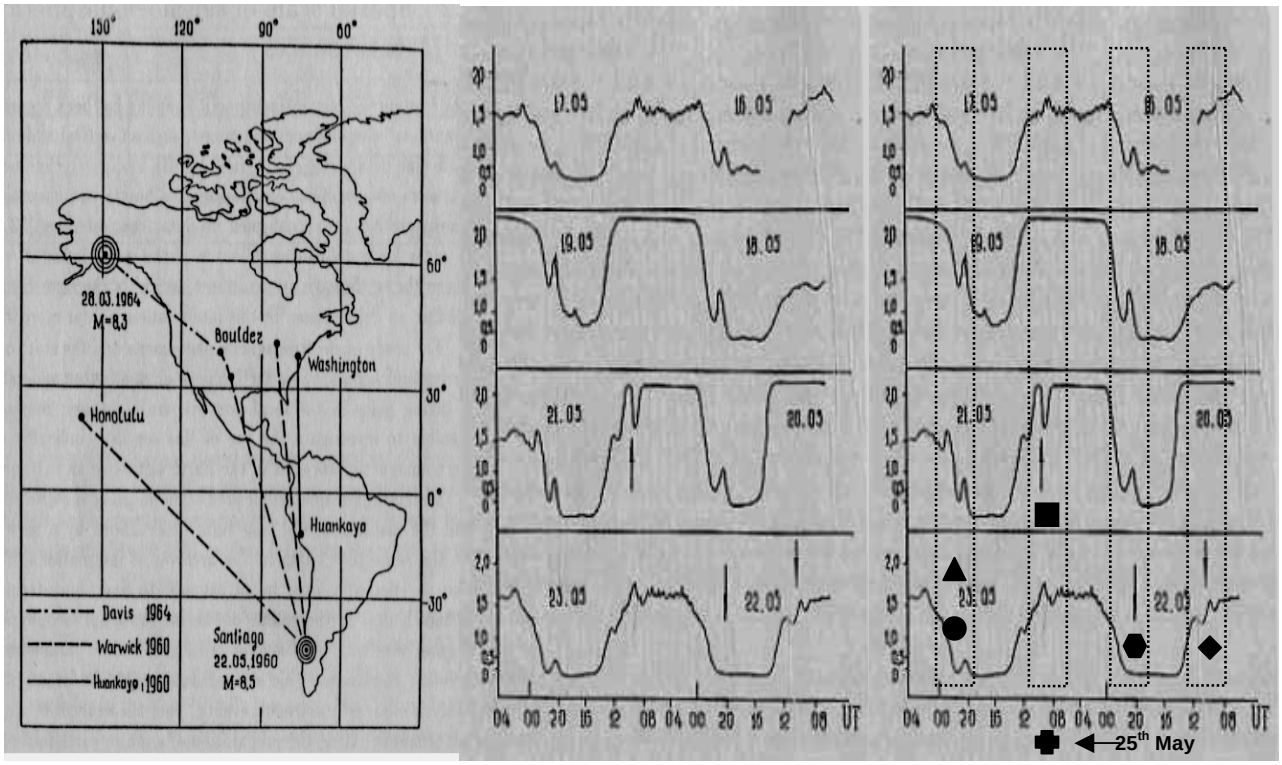

Part A *Part B.* *Part C*

Figure 4: Part A shows the relative positions of observation posts during the recording of anomalous effects of the Alaska earthquake of 28 March 1964, M = 8.3 and Chilean earthquake of 22 May 1960, M = 8.5.

Part B shows the recording of diurnal signal intensity envelopes (16-22 May 1960) at a frequency of 10 MHz on the Washington-Huankayo path prior to the disastrous quake in Chile. (NEIC, USGS have revised magnitudes to 9.2 and 9.5 for Alaska and Chile earthquakes, respectively.)

Part C shows the positions of earthquakes (as per table 3) by means of dots of different shapes.

(Parts A and B of the above diagram are reproduced with prior permission from a book on "EARTHQUAKE PREDICTION SEISMO-ELECTROMAGNETIC PHENOENA" by Gokhberg M.B., Morgounov, V.A. and Pokhotelov, O.A., from the Institute of Earth Physics, Russian Academy of Science, Moscow, Russia.)

Table 3: Major earthquakes in Chile during May 1960 as provided in the book (Gokhberg et al., 1995)

SR. NO.	DATE	TIME UT	MAGNITUDE	REMARK
01 ■	21.05.1960	10.02	7.2	Foreshock
02 ◆	22.05.1960	10.32	7.3	Foreshock
03 ⬢	22.05.1960	19.11	8.5	Main Shock
04 ●	23.05.1960	00.23	6.7	Aftershock
05 ▲	23.05.1960	00.25	6.8	Aftershock
06 ✚	25.05.1960	08.34	6.7	Aftershock

If one minutely observes these waveforms, similar anomalies were seen between 08-12 hours and 19-00 hours on almost all these days (17-23 May 1960). These anomalies are marked by two sets of vertical columns as illustrated in part C. The onset time of all foreshocks, main shock and aftershocks provided in table 3 also corresponds to the timing of these anomalies. The positions of six quakes are indicated by dots with different shapes.

It is evident from this table that high stresses occurred consistently at these times, which caused these anomalies and triggered all the six large magnitude earthquakes.

2.4 Example 4: EM noise of the atmospherics at the ORSOC

EM noise of the atmospherics at the ORSOC (Okayama Ridai Seismic Observatory Center) (E $144^0$55', N$34^0$41') and its neighborhood was measured using multiple antennas in the VHF band. To detect the direction of the locality of an earthquake, six yagi antennas pointing in six directions in an array of 12 FM tuners (Freq range 76-108 MHz) were used. The commercial broadcast frequencies were avoided. TDM (0.5 s switching, 10s rate) mode was used to detect the voltage corresponding to noise in the desired band. Sets of two channels were pointing in the directions of East, West, South, North, Ground, Heaven and Galaxy (Yamamoto et al., 2002). Typical multi-channel noise observed on 17 July 2001 is provided in Fig. 5. However the authors have not provided any correlation of this RF emission with any seismic activity. It is possible that there may not be any seismic activity in the region close to the monitoring at ORSOC.

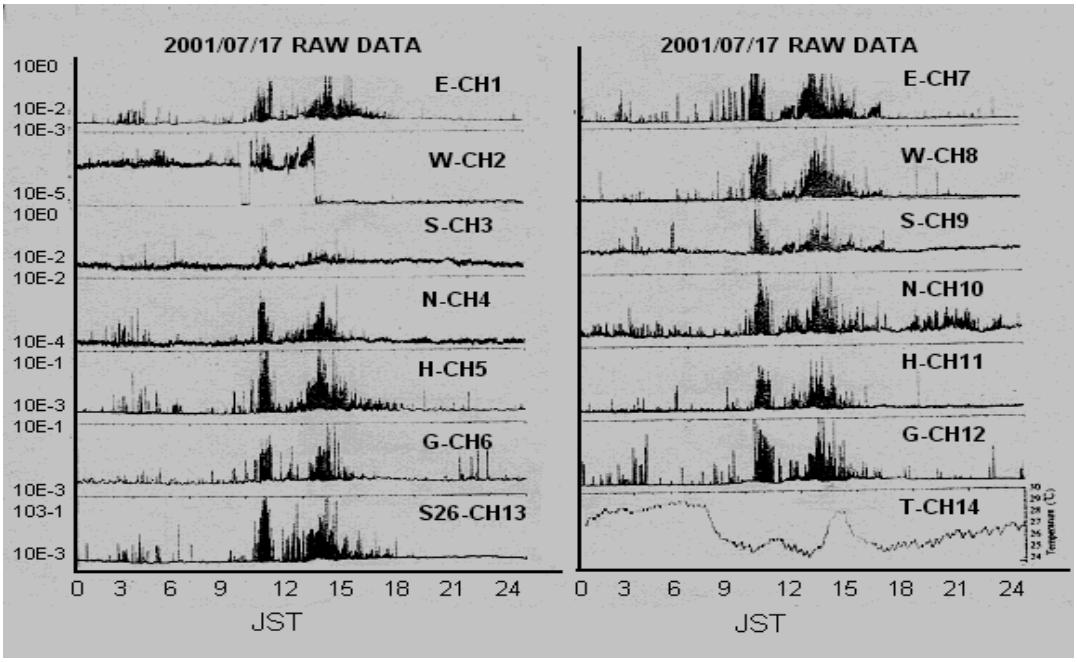

Figure 5: EM noise of the atmospherics at the ORSOC (Okayama Ridai Seismic Observatory Center, E 144-55'48.3, N34-41'48.1) and its neighborhood for 1-13 channel for 17 July 2001. Such signals were often recorded and confirmed throughout the summer season. The times of these RF emissions in VHF band fall on either side of the local noon period. (The times are provided in JST.)
(This figure is reproduced here (Yamamoto et al., 2002) with prior permission from the first author Dr. Isao Yamamoto.)

Table 4: Four events, which occurred close to the location of ORSOC, picked up from NEIC, USGS earthquake catalogs. Timings of the first and fourth events (of above table) seem to have occurred during the first and second of the semi-diurnal RF emissions, respectively.

YEAR	MONTH	DATE	HR:MN:SEC	LAT	LONG	MG	DEPTH
2001	07	17	22:47:39	39°43'N	141°34' E	4.6	85
2001	07	19	10:26:46	27°18' N	140°34' E	4.1	501
2001	07	19	21:02:36	36°13' N	139°67' E	4.9	74
2001	07	20	04:26:40	32°35' N	137°49' E	4.6	402

Four events indicated in table 4 (Source: NEIC-USGS) fall within a few hundred km of ORSOC, which occurred within three days of this type of RF emission (on 17 July 2001). Since a large part of the region in the vertical scale (longitude wise) would be under stresses at the time of RF emission, the earthquake could occur at those places which have seismically matured. Hence the earthquake epicenters could lie a few hundred km from the observatory center such as ORSOC.

It is seen from the timings of the first and fourth events (of table 4) that they seem to have occurred during the first and second of the semi-diurnal RF emissions (considering the +9 hour time difference between UT and JST). This is consistent with other examples in which seismic and volcanic activities were observed at the time of RF emissions.

2.5 Example 5: Kobe earthquake of 17 Jan. 1995

The sub-ionospheric VLF Omega signal transmitted from Tsushima (34°37'N, 129°27'E), Japan, is continuously received in Inubu (35°42'N, 140°52'E). The signal propagation characteristics (phase in particular) exhibited abnormal behavior (especially around the local sunrise and sunset times) a few days before the main shock of 17 Jan. 1995 (Haykawa et al., 1996). The authors indicate the sudden changes in these phases on 15 and 17 Jan. 1995, prior to the great Kobe earthquake. The phenomenon is illustrated in Fig 6. The times at which these VLF signals' phase reach minimum are again spaced equally from the local noontime. The Kobe earthquake occurs /occurred a couple of hours prior to the first VLF phase minimum.

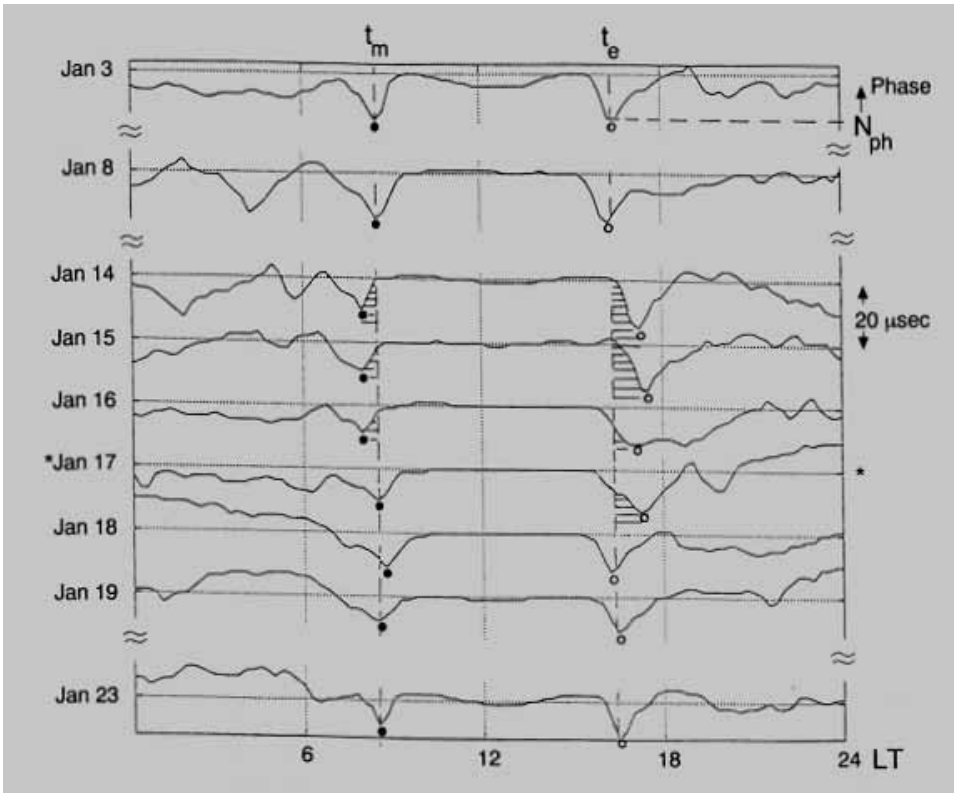

Fig. 6: Sequential plots of the diurnal variation of VLF signal (F = 10.2 kHz) phases observed at Inubo. Here t_m and t_e denote the time where the phase reaches a minimum around sunrise and sunset; the value of the phase of the phase minimum is defined as N_{ph}. The phase of each day is shown in the same relative units. (This figure is reproduced here from a paper (Hayakawa et al., 1996) with prior permission from the first author Prof. Hayakawa.)

2.6 Example 6: Observations from Apollo Lunar Seismic Experiment (APSE)

APSE consisted of four seismometers placed on the lunar surface during 1969-1972. Each station included three long period instruments and a vertical short period. The data was telemetered to earth and recorded until 1977. Deep moonquakes at the depth of 700-1000 km dominate the entire collection of data and show good correlation with the tidal stresses. It is seen from the record (arranged by synodic month) that the noisiest part of the record occurs close to the times of lunar sunrise and sunset, even accompanied with spikes. The three-day (solar day) offset in the time of sunrise/sunset (around 10 & 23 days from new Moon for station 12 and around 07 & 20 days from new Moon for station 16; station 12 and station 16 were commissioned during the Apollo 12 and Apollo 16 missions, respectively) reflects the 39 degree difference in the longitudes of the two stations. This indicates that the local noisy period is not simultaneous and varies with longitude. The pattern is similar to the semi-diurnal pattern seen on the earth at different longitudes. The power spectra of the moonquakes also show peaks corresponding to synodic month, which suggests occurrences of moonquakes during the noisy periods (Lammlein et al., 2005). Table 5 summarizes all the six examples discussed earlier.

3. GENERATION OF THE RF EMISSION ENVELOPE OBSERVED AT BHATSA

Fig. 1 shows the start and end portions of a typical RF disturbance (diurnal type) observed at Bhatsa prior to the Valsad earthquake sequence. If all these start and end portions of different links in the Bhatsa network are rearranged in order of their disturbance periods (which is inversely proportional to the received signal strength) then they provide an envelope of rising and falling emission signals as illustrated in Fig. 7. In this diurnal-type of RF emission, the signal strength of RF noise increased steadily (with increasing stress) knocking out different links at different times (based upon received signal strength of different station signals). Later, when this RF emission signal strength decreased steadily, it brought back the links with higher signal strength first, followed by other links with lower strengths in decreasing order.

Table 5. Details of all the six examples of semi-diurnal EM emissions spaced equally from the local noon timings.

EQ /VOLCANO SEQUENCE PLACE, PERIOD, FREQ-BAND OF EM EMISSION	TIMINGS OF THE SEMIDIURNAL EM EMISSIONS	LOCAL NOON TIME & TIME OFFSET OF EM EMISSIONS	REMARKS
Valsad, India. 10 –30 April 1991 UHF RANGE 460-461 MHz.	0400 GMT (0900 LT & 1200 GMT (1700 LT) Duration 10-100 min.	0800 GMT (1300 IST) Time offset = ± 4 hours	The times of the main shock 05:13 h (GMT) on 30-04-1991 and one of the two foreshocks 04:17 h (GMT) on 14.04.1991 closely match the time of the first RF emission. Semidiurnal type RF emission seized after the main shock.
Mt. Mihara Volcano, 03-21 Nov 1986 LF - 82 kHz	09 -11 hrs. JST 14 -16 hrs. JST	1230 hrs. JST Time offset = ±2.5 hours	1st eruption at 1725 hrs. JST, Nov 15, 1986 and 2nd eruption at 1615 hrs. JST, Nov 21, 1986, occurred at the times of the EM emissions.
Chilean Earthquake 16-23 May 1960 HF 10 & 18 MHz	08 -12 hrs. GMT & 19 -24 hrs. GMT	1700 hrs. GMT approx. Time offset = ± 5 hours	All six earthquakes (two foreshocks, main shock and three aftershocks) with magnitude range of 6.7 – 9.5 occurred within the times of RF emission.
ORSOC, Japan 17.07.2001 VHF 76-108 MHz	09 -11 hrs. JST 1230 -1430 JST	1200 hrs. JST approx. Time offset = ±1.5 hours	Four events occurred in the nearby area within three days of the occurrence of RF emission. The times of two of them match the times of RF emission.
VLF sub-ionospheric signals **[Kobe quake]** VLF range Jan 03-23,1995 10.2 & 11.3 kHz	0830 hours JST & 1630 hours JST	12-30 hrs. JST (Timings of the VLF phase reaching minimum) Time offset = ± 4.0 hours	The times when these VLF signals' phase reaches minimum are spaced equally from the local noon time. Kobe earthquake timings (0546 hrs) differ by a couple of hours from the first VLF phase min. timing.
Apollo Lunar Seismic data for stations 12 and 16 (1969 -1977) Microwave range 1-2 GHz	Around 10 & 23 days from new Moon (station 12) Around 07 & 20 days from new Moon (station 16)	Around 16.5 days from new Moon (Station 12) Around 13.5 days from new Moon (Station 16)	Three-day offset in the occurrences of EM emissions at these places reflects the 39 degree difference in the longitudes of the two stations. The power spectra of the moonquakes show smaller peaks corresponding to synodic month, which suggest occurrences of moonquakes during the noisy periods (Lammlein, 1977)

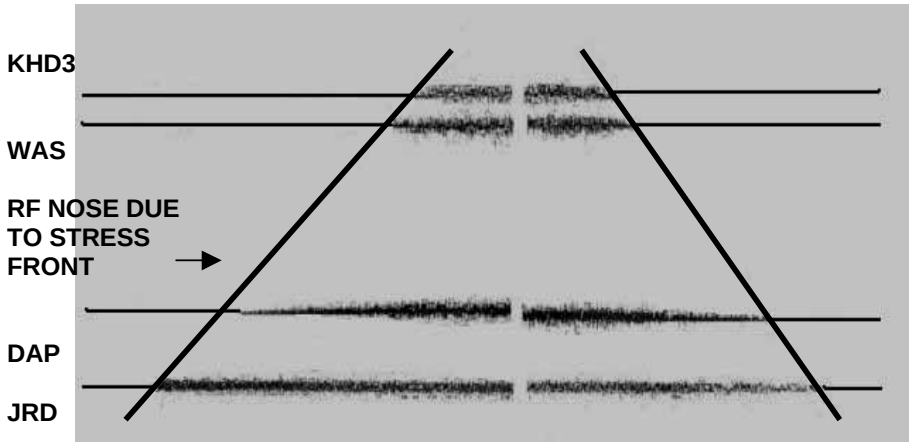

Figure 7. Start and end portions of the signals for different links in the Bhatsa net are rearranged in terms of the received signal strength, which provides an envelope of rising and falling RF emission signals. The other channel links (BIR, BHT, AJP, DLK) show noise of much shorter duration and hence those corresponding noise portions do not figure in this diagram. The KHD stations had three axial seismic sensors and hence the durations of noise portions were identical for all three signals from this station.

4. MONITORING THE LOCAL STRESS FRONTS

A grid of UHF/VHF links can be used to monitor the strength of various stress fronts in the seismically active region, which can provide warning of the impending earthquakes. A typical arrangement is illustrated in Fig. 8. As illustrated in this figure, a set of four receivers at the location of every medium size dot will receive signals from four transmitters located at four corners of a square of size 50 km x 50 km and operated at different spot frequencies in the UHF/VHF band. The transmission can be through an omni-directional antenna since receivers in the adjacent block can monitor the same signal. The receivers are provided with different sets of attenuators so that their sensitivity settings are different.

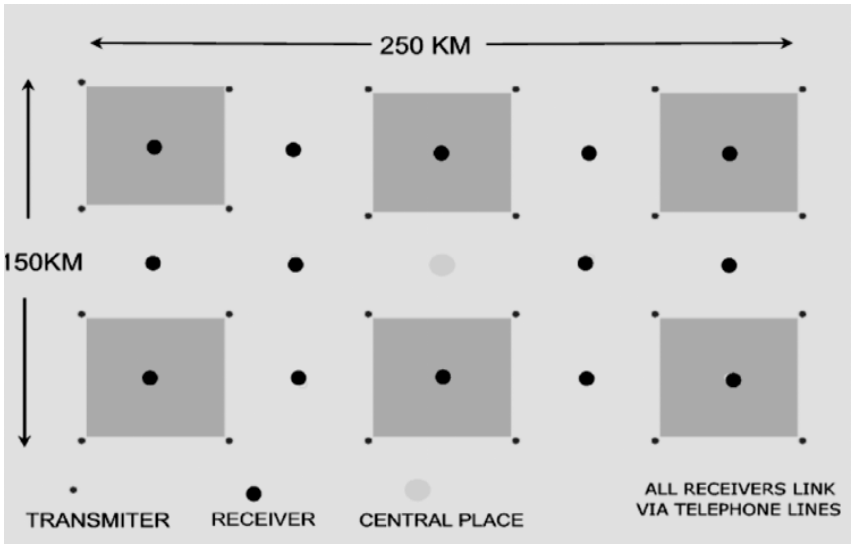

Fig. 8. Grid of UHF/VHF links for monitoring high-seismicity region.

On a daily basis, the RF noise envelope due to the stress front (semidiurnal type) would rise by about 10-15 dB, which would result in at least one of the receivers (with maximum input attenuation) generating a noisy signal. The rocks under stress would emit higher RF noise just before they reach breaking point (Ogawa, et al., 1989; Sachiko, T. et al., 2002) and can sound the alarm for an impending earthquake in the close vicinity. This higher RF noise envelope can be witnessed (on a daily basis) for a few days before the impending earthquake.

This direct RF noise measurement in the UHF/VHF bands can also be carried out using the multi-channel system adopted (Yamatoto et al., 2002). The utilization of the HF band (as in the case of Chilean earthquakes) could

broaden the technique for use in the detection of precursors of normal and deep-focus earthquakes from tele-distances. The technique can be used effectively for monitoring large areas.

5. DISCUSSION

5.1. EM emission related to earthquakes and volcanoes

It is believed that the RF emissions come directly from the crystalline rocks of the crust. These rocks provide some sort of piezoelectric effect when subjected to stress.

In the semidiurnal type of RF emission, stresses were consistently seen twice a day, spaced equally on either side of the midday timings. A similar effect is seen on the surface of the moon (synodic month) and both these phenomena are caused by the Sun's position. This is a daily phenomenon and the rise in the intensity of the EM emission, by about 10-15 dB (-146 dB to about - 130dB) is observed on a daily basis. However the same amount of stresses provide much higher EM noise from the region, matured for earthquakes. Earthquakes/volcanic eruptions were consistently found during these EM emissions, which is the result of the stresses created.

The six examples provided prove that the emission was observed in a broad frequency band from VLF to Microwave range. The application of semi-diurnal stresses, which results in RF emission, does not seem to be a local phenomenon. The entire rock under stress in the vertical column (several km wide) could contribute to EM emission.

The types of emission observed at Bhatsa and also observed at other places (with regard to Chilean earthquakes and eruption of Mt Mihara Volcano) do correlate with the rotation of the earth. Occurrences of moonquakes have also provided a direct correlation with the rotation of the moon. FFT spectra of the moonquakes show major peaks at 50 and 100% of the sidereal phase (13.6 and 27.2 days). However the same FFT spectra provide a smaller peak corresponding to the synodic month, indicating moonquakes taking place during the semidiurnal stresses generated by the Sun in synodic phase (Lammlein et al, 1977). This semi-diurnal RF emission observed on a daily basis does not provide any correlation with the lunar tidal forces, which is considered as another triggering source for earthquakes (Sachiko et al., 2002).

The EM emission in the UHF band was witnessed for about two months even after the Valsad earthquake sequence. This is possible when most stored energy is released in the form of earthquakes, the region may continue to provide EM emission at a lower level. This is seen in many other examples (Hata et al.).

5.2. Study of temporal and spatial variation of the time-offsets

In the six examples shown in table 1, the timings of semidiurnal emission show different time-offsets (displacements) from the local noontime of between ± 1.5 hours and ± 5 hours. At Bhatsa seismic telenet it was observed that this time-offset is not fixed. Although it does not vary on a day-to-day basis, it does indicate different timings for different periods. During the Valsad earthquake sequence of April 1991, it was found to be ± 4 hours while in the helical record of July 1993, the time-offset was found to be ± 6 hours.

Continuous data of synodic phase versus occurrence time of RF emission for stations 12 and 16 [Apollo Lunar Experiment], in which the maximum amplitude is associated with RF spikes, exhibit a sinusoidal behavior consistent with the varying length of the lunar synodic month (Bullow et al., 2005). Similar behavior is also witnessed in the timings of temporal variation of monthly average values of "tm" and "te" for phase and amplitude of the VLF signal, which shows good correlation with the varying day period from October to April (1995) at Inubu, Japan (Hayakawa et al., 1996).

The other four cases are different than the above two examples and in general the temporal and spatial variation in these time-offsets with respect to the local noontime need to be studied systematically, which will provide some clues about the cause of such stresses being built within the body of the earth.

5.3. Possible causes of the diurnal type of EM emission

It was observed in cases of semidiurnal-type emissions that the Sun could be instrumental in generating the stresses on earth. Similarly, in the case of diurnal-type emissions, considering their consistent timings, again some external forces could be responsible for these phenomena. These external forces may possibly be caused by planetary position (Li, 2006; Venkatnathan et al, 2005). During the intense RF emission of the diurnal type observed at Bhatsa (for about a week at certain times of the day some three weeks prior to the Valsad earthquake sequence), this (Valsad) portion of the globe would see the same planetary position. The steady increase and decrease of RF emission could be due to the rotation of the Earth, which brought this earthquake region to face a certain planet position and then steadily moved away from it. However, more such examples are needed to confirm the possible causes of diurnal-type emission.

5.4 Possible event sequence, resulting in an earthquake

At Bhatsa, the timings of diurnal-type RF emissions (at 00 h GMT) and those of semidiurnal-type (at 0400 and 1200 h GMT) were different. Also the EM emission in a diurnal pattern was more intense. In the case of the Chilean earthquake of 22 May 1960 (*Mb* = 9.5), Warwick et al. (1982) provided the details of radio noise at 18 MHz on 16 May 1960 between 0350 GMT and 0410 GMT, six days prior to the great earthquake. This timing is again different than those of the semidiurnal type (listed in Table 1). In both cases (Bhatsa and Chilean earthquakes) diurnal-type emissions led to semidiurnal-type emissions.

Most earthquakes occur within 3 days of formation of diurnal type stresses (Venkatnathan et al., 2005). In several instances the occurrence of the earthquake is not instantaneous and these diurnal type stresses would make this earthquake-prone area more vulnerable. As seen in the above examples, during the application of semi-diurnal stresses acting on a daily basis, the region shows higher emission of RF noise. The phenomenon continues for a few days and subsequently results in the occurrence of earthquakes during the application of one such semidiurnal stress.

6. Conclusions

EM emission related to earthquakes and volcanoes is a broadband phenomenon. This is broadly found in two versions, diurnal and semidiurnal type. Diurnal-type emissions are found to be more intense than the semidiurnal type. The timings of semidiurnal-type emissions are spaced equally on either side of the local noontime. The occurrences of earthquakes/volcanic eruptions are simultaneous with the emission times indicating that some stresses are generated during these periods. The causes of semidiurnal stresses seem to be the position of Sun. The causes of diurnal-type emission could be the planetary alignment, but more such cases need to be sought and examined to draw a precise conclusion.

Acknowledgements: I am grateful to Prof. Hayakawa and Prof. Yamamoto for permitting the use of figures from their papers and Prof. Gokhberg for permitting the use of a figure on the Chilean earthquake from his book. Illustration of these figures was very crucial in the context of this article. I am also grateful to Dr. R.S. Chaughule, Dr. S.L. Wadekar and Dr. M. Ramanmoorthy for various discussions on the manuscript of this article.

References

Bulow, R.C., Johnson, C.L. and Shearer, P.M., (2005). New events discovered in the Apollo Lunar Seismic Data. *Journal of Geophysical Research*, v. 110, E10003, doi:10.1029/2005 5JE002414,2005.

Gokhberg, M.B., Morgounov, V.A., and Pokhotelov, O.A., 1995. Earthquake Prediction Seismo-electromagnetic Phenomena. Gorden and Breach Science Publication, p. 112-113.

Hata, M., Takumi, I., Yahashi, S. and Yasukawa, H. Electronic Wave radiation due to the possible plate slip at the central Shizuoka Earthquake and to the Island Diastrophism and Volcanic Eruption in Miyake Island, www.ursi.org/Proceedings/ProcGA02/papers/p0661.pdf

Hayakawa, M, Molchanov, O.A, Ondoh, T. and Kawai, E, 1996. The precursory signature effect of the Kobe earthquake of VLF sub-ionospheric signals. *Journal of the Communication research laboratory*, v. 43, p. 169-180.

Kolvankar, V.G., Nadre, V.N., Arora, S.K. and Rao, D.S., 1992. Development and deployment of radio telemetered seismic network at Bhatsa. *Current Science*'s special issue on "*Seismology in India - an overview*", v. 62, p. 199-212.

Kolvankar, V.G., 2001. Earthquake Sequence of 1991 from Valsad Region, Guajrat. BARC-2001/E/006.

Lammlein, D.R., 1977. Lunar seismicity and tectonics. *Physics of the Earth and Planetary Interiors*, v. 14, p. 224-273.

Li, Y., 2006. An examination of the correlation between earthquake, positions of solar system bodies and solid tide. *Science in China: Series G Physics, Mechanics & Astronomy*, v. 49, no. 3, p. 367-376. DOI 10.1007/s11433-006-0367-x.

Ogawa, T., Oike, K. and Miura, T., 1985. Electromagnetic radiation from the rock. *Journal of Geophysical Research*, v. 90, p. 6245-6249.

Sachiko, T., Masakazu, O. and Haruo, S., 2002. Evidences for tidal triggering of earthquakes as revealed from statistical analysis of global data. *Journal of Geophysical Research*, v. 107, No. B10, 2211 doi:10. 1029/2001 JB001577.

Venkatanathan, N., Rajeshwara Rao, N., Sharma, K.K. and Periakal, P., 2005. Planetary Configuration: Implication for earthquake prediction and Occurrences in South Peninsular India. *Journal of Indian Geophysical Union*, v. 9, p. 263-276.

Yamada, I., Masuda, K. and Mizutani, H., 1989. Electromagnetic and acoustic emission associated with rock fracture. *Physics of the Earth and Planetary Interiors*, v. 57, p. 157-168.

Yamamoto, I., Kuga, K., Okabayashi, T. and Takashi, A., 2002. System for earthquake prediction research in the region of VHF frequency band. *Journal of Atmospheric Electricity*, v. 22, p. 267-275.

Yoshino, T. and Tomizawa, I., 1989. Observation of low frequency electromagnetic emissions at precursors to the volcanic eruptions at Mt. Mihara during November 1986. *Physics of the Earth and Planetary Interiors*, v. 57, p. 32-39.

Warwick, J.W., Stoker, C. and Meyer, T.R., 1982. Radio emission associated with rock fracture: Possible application to the Great Chilean earthquake of May 22, 1960. *Journal of Geophysical Research*, v. 87, p. 2851-2859.